Appl Phys A (2013) 113:905–910
DOI 10.1007/s00339-013-7721-4

Applied Physics A
Materials Science & Processing

A Roman bronze statuette with gilded silver mask from Sardinia: an EDXRF study

Roberto Cesareo · Antonio Brunetti · Rubens D'Oriano · Alba Canu · Gonaria Mattia Demontis · Angela Celauro

Received: 15 April 2013 / Accepted: 19 April 2013 / Published online: 3 May 2013

Abstract A Roman bronze statuette from the 2nd Century BC was recovered from a nuragic sanctuary close to Florinas, in the north of Sardinia. The facial portion of the statuette is covered by a silver mask, partially gilded and attached to the bronze by tin-lead welding.

The silver mask was carefully analyzed by portable energy-dispersive X-ray fluorescence (EDXRF), a non-destructive and non-invasive method. The aim of the analysis was to reconstruct the layered structure of the silver gilt mask, and to determine homogeneity and thickness of the gold, silver and lead–tin sheets. This is possible by using the internal ratio of the X-ray lines, i.e. starting from the surface, Au (Lα/Lβ), Ag (Kα/Kβ), Au-Lα/Ag-Kα and Pb (Lα/Lβ).The results were compared with those obtained with simulated X-ray spectra, obtained both experimentally and by using the Monte Carlo simulation technique.

R. Cesareo (✉)
Istituto per lo Studio dei Materiali Nanostrutturati, CNR-Montelibretti, via Salaria km. 29.5, Monterotondo, 00015 Rome, Italy
e-mail: cesareo@uniss.it

A. Brunetti
Dipartimento di Scienze Politiche, Scienza della Comunicazione e Ingegneria dell' Informazione, Universitá di Sassari, Sassari, Italy

R. D'Oriano
Soprintendenza per i Beni Archeologici, Sassari, Cagliari, Italy

A. Canu · G.M. Demontis
Centro di Restauro della Soprintendenza per i Beni Archeologici, Sassari, Cagliari, Italy

A. Celauro
Dipartimento di Scienze della Terra, Università di Roma 'La Sapienza', Rome, Italy

1 Introduction

A bronze statuette was recovered from the nuragic sanctuary of Giorrè, close to Florinas, in the north of Sardinia (Fig. 1): this nuragic settlement is made up of several rooms surrounded by a wall of which at least one of them may be connected with the cult of the water [1].

Unfortunately, the context data referable to the little statue are scarce and approximate because this area has been

Fig. 1 Map of the north-west side of Sardinia. Close to the town of Florinas, province of Sassari, which is shown in red, there was recovered the statuette shown in Fig. 2

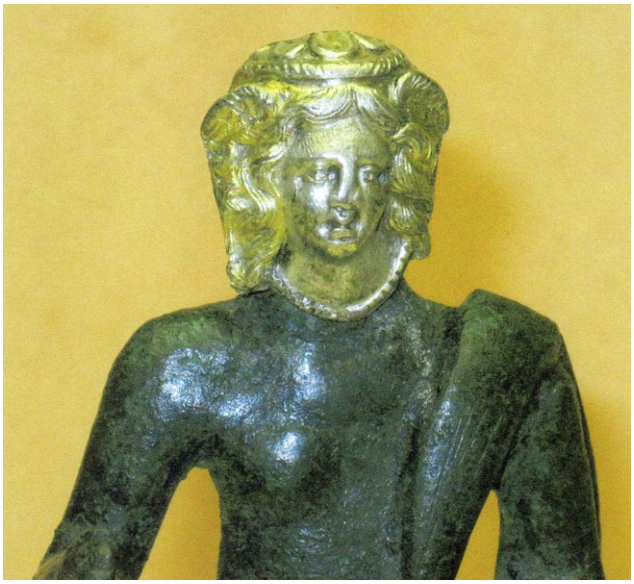

Fig. 2 Bronze statuette with silver gilt mask from the 2nd Century BC, recovered from the nuragic sanctuary of Giorrè, close to Florinas, in the north-west of Sardinia

illegally excavated before the official archaeological dig: in fact, the statuette was found in the area subjected to illegal excavation, together with fragments of a ceramic plate dated to the second century BC, and some Punic coins of local and Siceliot brand dating to the fourth and third centuries BC, which are the only recognizable findings of historical times recovered from the excavation.

The bronze statuette is 14 cm tall and represents a naked standing figure whose typology may recall the models of the Greek sculptor Praxiteles.

The silver mask (Fig. 2), which shows traces of gilding on its hair, is indicatively dated, on stylistic grounds, after the middle of the second century BC. It was originally a decorative element of another object, as is testified by the presence of the rosette-shaped decoration in the upper part of the mask, from which it was cut; the would-be mask was then applied on the face of the figure, which, as shown by the radiographs performed on the piece, had not been outlined [1]. Therefore, the statue was made from the start with the intention of applying the silver mask on the face area.

The presence in the mask of wings between the hair is the element that may suggest an image of Hermes, Medusa or, with less probability, Perseus or one of the Gods representing the winds. In the intentions of the person who commissioned the making of the artefact, the statuette was probably intended as a representation of Hermes, a mythological figure certainly better known than Perseus or Medusa or Wind-God, especially in an inner area of Sardinia during the second century BC.

This deity has multiple connections with the cult of the water; this case should therefore be interpreted with a persistence of the worship of water in salutary function attested in geographical areas not far from Florinas (Thiesi—Monte Ruju; Romana—Santu Giolzi) in places and with votive offerings classifiable in the same historical context. That would signify, in this case, the survival of an older cult in the sanctuary in the same chronological period.

It can be proposed that the cultural environment connected with this production is that of the local culture, in other words the populations of mixed Punic and indigenous extraction who, in this area of Sardinia in the second century BC, are mainly related to working the land.

There are no known comparisons with this statue in Sardinia and elsewhere, so that this find seems to be an unique one. The aim of this study was to study the layering structure of the mask.

2 Methods

Analysis of X-ray spectra of multilayered structures, such as the mask of this statuette (Fig. 2), allows us to obtain information about composition and thickness of the various layers, due to various self-attenuation and attenuation effects[1] [2–6]. In fact, starting from the surface analysis of the mask (Fig. 3) the following data can be obtained:

- **Au Lα/Lβ**: this ratio allows us to determine the gold leaf thickness d, according to

$$\mathrm{Au}\left(\frac{\mathrm{L}_\alpha}{\mathrm{L}_\beta}\right) = 0.735\left(\frac{1-\mathrm{e}^{-3900d}}{1-\mathrm{e}^{-2860d}}\right). \tag{1}$$

- **Ag Kα/Kβ**: this ratio allows us to determine the silver layer thickness d, according to

$$\mathrm{Ag}\left(\frac{\mathrm{K}\alpha}{\mathrm{K}\beta}\right) = 0.925\left(\frac{1-\mathrm{e}^{-530d}}{1-\mathrm{e}^{-490d}}\right) \tag{2}$$

and considering the Au attenuation effect, according to

$$\mathrm{Ag}\left(\frac{\mathrm{K}\alpha}{\mathrm{K}\beta}\right) = 0.925\left(\frac{1-\mathrm{e}^{-530d}}{1-\mathrm{e}^{-490d}}\right)\mathrm{e}^{-322d(\mathrm{Au})}. \tag{3}$$

- **Au Lα/Ag Kα**: this ratio allows us to determine the gold leaf thickness, according to

$$\frac{N(\mathrm{Au})}{N(\mathrm{Ag})} = P\left[1-\mathrm{e}^{-2885d(\mathrm{Au})}\right]\mathrm{e}^{-1598d(\mathrm{Au})}, \tag{4}$$

where P is a parameter to be determined experimentally.

- **Pb $\mathrm{L}_\alpha/\mathrm{L}_\beta$**: to obtain information about the Pb thickness, according to

$$\mathrm{Pb}\left(\frac{\mathrm{L}\alpha}{\mathrm{L}\beta}\right) = 0.75\left(\frac{1-\mathrm{e}^{-1630d}}{1-\mathrm{e}^{-1180d}}\right)\mathrm{e}^{-422d(\mathrm{Ag})}\mathrm{e}^{+1100d(\mathrm{Au})}. \tag{5}$$

[1] The theoretical basis for self-attenuation and attenuation effects is described in Refs. [2–6].

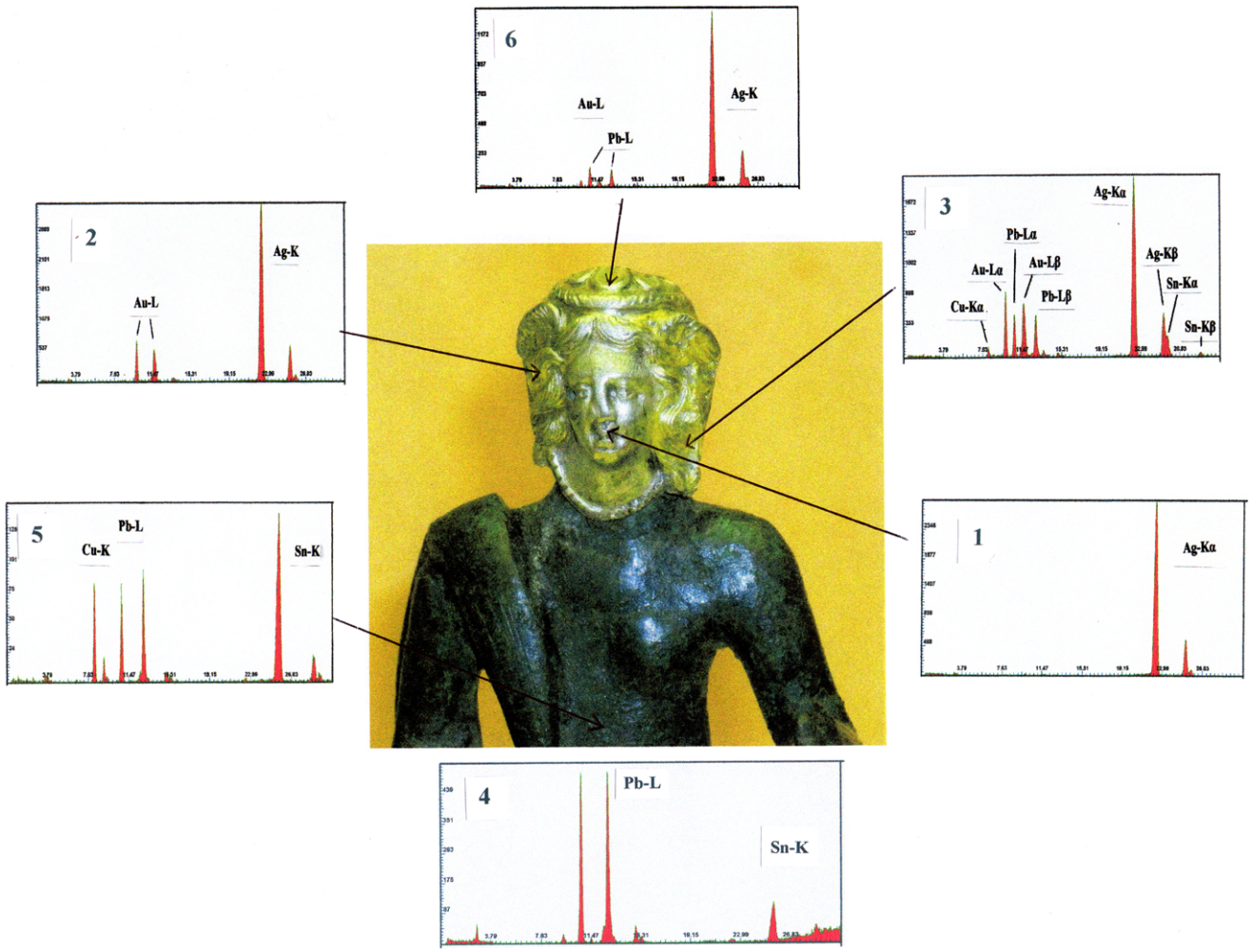

Fig. 3 Energy-dispersive X-ray fluorescence spectra of various areas of the statue and of the mask. The following areas were analyzed: *1*. Nose, mouth and cheek; *2*. Hair (right-hand side); *3*. Hair (left-hand side on the bottom); *4*. Small quantity of powder taken from the interface silver–bronze; *5*. Bronze, front side (stomach); *6*. Hair (on the top of the head)

– **Pb L_α/Sn K_α**: to obtain information about the tin-lead layer composition, according to Eqs. (6a), (6b):

$$\mathrm{Pb}(L_\alpha) \cong N(\mathrm{Pb})\mathrm{e}^{-1675d(\mathrm{Ag})}\mathrm{e}^{-2540d(\mathrm{Au})} \times \sigma_{\mathrm{ph}}(\mathrm{Pb})\omega(\mathrm{Pb})\varepsilon(\mathrm{Pb}) \quad (6a)$$

and

$$\mathrm{Sn}(\mathrm{K}\alpha) \cong N(\mathrm{Sn})\mathrm{e}^{-485d(\mathrm{Ag})}\mathrm{e}^{-1680d(\mathrm{Au})} \times \sigma_{\mathrm{ph}}(\mathrm{Sn})\omega(\mathrm{Sn})\varepsilon(\mathrm{Sn}), \quad (6b)$$

which correspond to the net counts of Pb and Sn in the detector.

3 Energy-dispersive X-ray fluorescence (EDXRF): features and experimental set-up

The portable equipment employed for the analysis of the statuette is composed of a mini X-ray tube [7, 8] with a Ag anode, working at 40 kV and 200 μA maximum voltage and current, and of a 123 Si-drift detector with related electronics (Fig. 4) [9]. This portable EDXRF equipment irradiates and analyzes areas of about 5 mm diameter, when the object is at a distance of a few cm; the X-ray tube output is filtered and collimated. The radiation protection problem is negligible. The specifics of the Si-drift detector are as follows:

– **Si drift**: it is a thermoelectrically cooled detector, with 500 μm thickness and 7 mm^2 area of the Si crystal, and a thin Be window, of 12.5 μm with about 125–150 eV energy resolution at 6.4 keV. This detector has an efficiency of 97 %, 39 % and 14 % at 10, 20 and 30 keV, respectively.

Standard gold alloys, containing known concentrations of gold, silver and copper, and standard silver alloys, containing known concentrations of silver and copper, were employed for calibration. The peak areas have been extracted by using a genetic algorithm technique [10].

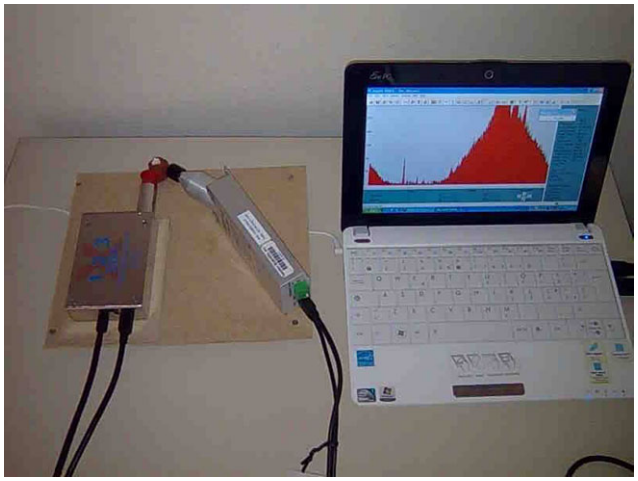

Fig. 4 Portable EDXRF equipment, composed of a Si-drift detector (450 μm thickness, 7 mm^2 area and 40 eV energy resolution at 5.9 keV) and an X-ray tube (40 kV and 100 μA maximum voltage and current and Ag anode). Electronics, including bias supply and multi channel analyzer (MCA), are in the case of the 123 SDD module

To measure gilding thickness of the silver gilt mask, the Au (Lα/Lβ), Ag (Kα/Kβ) and Au-Lα/Ag-Kα ratios were employed. To simulate the experimental situations, gold leaves were employed (each Au foil 0.125 μm thick) and silver foils (each Ag foil 0.28 μm thick). Also, calibrated Au leaves and silver sheets were employed.

A survey of analytical techniques for the study of multilayered samples can be found in Ingo et al. [11].

4 Results and discussion

On the basis of Eqs. (1)–(5) and X-ray spectra of the various parts of the mask (see also Fig. 3), the following parameters could be obtained:

1. *Area apparently free from gilding (nose, mouth and left cheek, Fig. 3, area 1)*:
   From the XRF spectra only the Ag lines are visible, with traces of Cu, Au and Pb at concentrations <0.5 %; X-rays from underlying Pb–Sn are not visible, and this fact gives a lower limit to the Ag thickness; from Eq. (2) and from the ratio Ag (Kα/Kβ) = 5.15 ± 0.2 (the same ratio for an infinitely thick Ag sample = 4.94), there turns out a mean Ag thickness = 80 ± 30 μm; in a successive measurement d_{Ag} = 120 ± 40 μm. The presence of traces of Au and Cu may depend on the fact that originally also the nose and cheeks were gilded; the presence of traces of Pb could be linked to the use of a Ag–Pb alloy.
2. *Hair, right-hand side of the head (Fig. 3, area 2)*:
   From the XRF spectra only the Ag-K and Au-L lines are visible (traces of Cu and Pb are also visible at concentrations <0.5 %); X-rays from underlying Pb–Sn are not detected at the correct concentration, and this fact again gives a lower limit to the Ag + Au thickness; from Eq. (1) and from the ratio Au (Lα/Lβ) = 0.82 a Au thickness of about 2.5 ± 0.5 μm can be deduced. Further, from the Ag (Kα/Kβ)ratio = 5.4 ± 0.2 there can be deduced a Ag thickness of about 80 μm. The presence of a very small Cu peak is not easy to explain; it cannot originate from the bronze, because the Cu transmission factor from Ag + Au would be $\exp(-2200 d_{Ag})\exp(-4000 d_{Au}) \sim 0$. On the other hand, it is not correlated with Ag, because of its lack in the silver X-ray spectrum (see Fig. 2, right on the bottom). The Cu peak could be ascribed to the gilding (Au + Cu alloy) or, at least partially, to contamination from the X-ray tube. If the first hypothesis is true, then an alloy composed of 90 % Au + 10 % Cu may be calculated.
3. *Hair, left-hand side of the head (Fig. 3, area 3)*:
   The X-ray spectrum is complex, and shows the presence of Cu, Au, Pb, Ag and Sn peaks. From the measurement of Au (Lα/Lβ) = 0.80 (Au ratio for infinitely thin sample = 0.93, for thick samples = 0.70) the gold thickness can be determined as d_{Au} = 3.0 ± 1.0 μm.

   From the ratio Au-Lα/Ag-Kα = 0.2, a gold thickness of about 1.7 ± 0.5 μm can be determined, whereas for the Ag thickness is about 10 μm.

   From the simulated XRF spectra the gold thickness fitting the experimental data gives the best result for d_{Au} = 1 μm.

   From all data a mean value for the gold thickness is d_{Au} = 1.7 ± 0.8 μm.

   The ratio Pb (Lα/Lβ) varies because of the Ag attenuation and because of the Au amplification (Fig. 5), according to the factors $0.75e^{-322 d(Ag)}e^{1100 d(Au)} = 0.8$ for a thickness of 20 μm Pb, of 8 μm Ag and of 3 μm Au, while the experimental value is 0.83 ± 0.04.

   Further, from the ratio Pb-Lα/Sn-Kα ∼ 1.25 the Ag thickness can be approximately evaluated, from Eq. (5), giving the value $d_{Ag} \sim 10$ μm (in the other analyzed areas where both Pb and Sn are present the Ag thickness was determined to be 10 μm for the right-hand side of the hair, and 7 μm in the head position).
4. *Analysis of a small quantity of powdered material taken mainly from the interface between bronze and silver mask (Fig. 3, area 4)*:
   From the X-ray spectrum of the powder it can be deduced that the welding is composed of a Pb–Sn alloy. The presence of a small Ag peak is due to the fact that the powder contains also silver from the mask.
5. *Bronze (stomach, Fig. 3, area 5)*:
   The XRF spectrum of the bronze, taken from an area with patina (it was out of the question to clean a small surface area) shows the presence of X-ray peaks of Cu, Pb and Sn of similar intensities. The only possible deduction is that

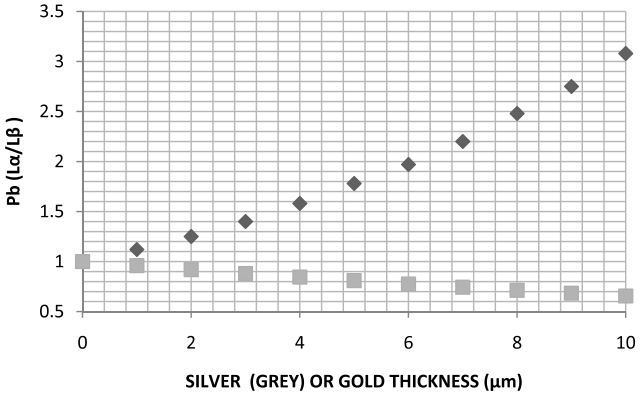

Fig. 5 Pb (Lα/Lβ) attenuated by silver sheets or amplified by gold leaves, both in μm

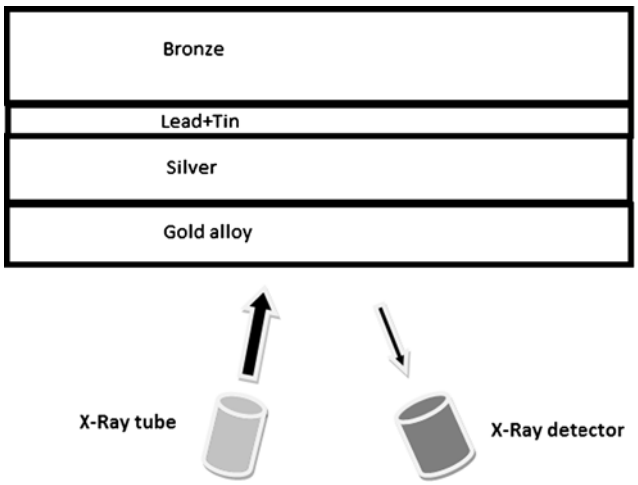

Fig. 6 Schematic view of the gilded silver mask superimposed with a Sn–Pb welding to the bronze statue. Bronze layer: lead and tin alloy (thickness of about 20–100 μm); silver layer: variable thickness (between 7 and 100 μm); traces of Pb (<0.5 %); gold layer: Au of variable thickness (between 1 and 5 μm); traces of Cu (∼10 %) and Ag at low concentration

the bronze is composed of Cu, with high concentrations of Pb and Sn, also considering that patina is generally enriched in Pb and Sn.

6. *Hair (on the top of the head, Fig. 3, area 6)*:
   From the ratio Au (Lα/Lβ) $= 0.88 \pm 0.05$ there may be calculated a Au thickness $d_{Au} = 1.3 \pm 0.6$ μm, and from the ratio Au-Lα/Ag-K$\alpha = 0.03$, $d_{\mathrm{Au}} = 1.2 \pm 0.5$ μm.

   From the ratio Pb (Lα/Lβ) $= 0.85 \pm 0.03$ and from Eq. (5), $d_{\mathrm{Pb}} = 8 \pm 1$ μm if $d_{\mathrm{Au}} = 1.5$ μm.

An approximate reconstruction of the silver mask over the bronze is finally shown in Fig. 6, and may be described in the following manner, starting from the surface:

– **GOLD:** forehead, hair and chin are gilded, and thicknesses of both the silver sheet and the gilding are variable;

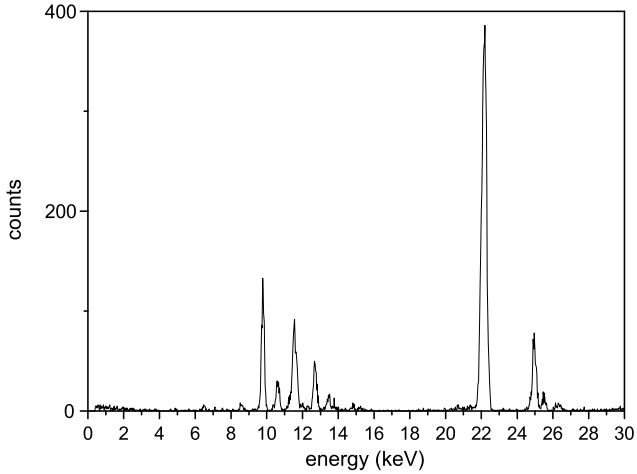

Fig. 7 EDXRF spectrum obtained with a simulated sample composed of a Pb–Sn sheet, a Ag foil of 8 micron thickness and a Au leaf of 1 micron. This spectrum can be compared with X-ray spectrum no. 3 of Fig. 3 and that of Fig. 8

– **SILVER:** the silver mask is free from gilding in the front region (eyes, nose and mouth); the silver thickness is variable;
– **LEAD–TIN ALLOY:** the welding is composed of a tin-lead alloy (approximately 50 % Sn and 50 % Pb);
– **BRONZE:** the bronze is rich in tin and lead. Because of the presence of patina it is difficult to give an exact composition, also because the related X-ray spectra change largely across the sample; in any case the Pb content reaches a maximum on the back of the statue.

A quality control of the results obtained was carried out by performing XRF measurements on samples formed by a sequence of layers with the same estimated thickness and composition. Figure 7 shows the XRF spectrum of the artificial multilayered structures corresponding to the area 3 of the mask.

Finally, the same spectrum was also simulated using a Monte Carlo program (Fig. 8), which is a fast XRF Monte Carlo simulation code [12]. It is based on an intensive use of variance-reduction techniques and uses a constantly updated X-ray library [13, 14]. It has been tested on various types of cultural heritage samples [15–19]. Besides its speed it has another unique, to the best of our knowledge, capability: simulation of arbitrarily rough surfaces. The rough surface condition is often found in cultural heritage samples, where the surface cannot be obviously smoothed. In Fig. 8 the simulated spectrum is superimposed to the experimental one.

From this simulation a thickness of 1 μm for Au and 7.5 μm for Ag layers can be estimated, and a Sn–Pb alloy composition of respectively 55 % and 45 % can be deduced, however with an uncertainty of about 10 %.

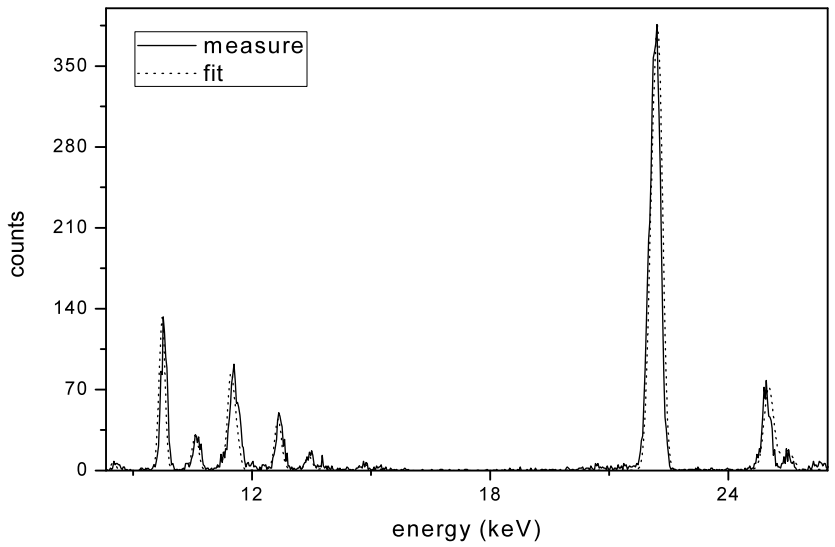

Fig. 8 Measured and Monte Carlo simulated EDXRF spectra of area 3 in Fig. 3 and with the spectrum of Fig. 7, assuming conditions $d_{Ag} = 7.5$ μm and $d_{Au} = 1$ μm

5 Conclusions

The analysis of the silver mask from the Roman statuette by energy-dispersive X-ray fluorescence gives a very clear example of how a multilayered sample can be reconstructed (in terms of composition and thickness of the various layers) by an accurate analysis of the intensity ratios of the various X-ray peaks. This suggests a completely new method to carry out EDXRF analysis and to process the X-ray spectra, i.e.

- analysis should give rise to X-ray peaks statistically relevant; for example, when the Cu (K_α/K_β) ratio will be successively employed for multilayered reconstruction, then the K_β peak must be characterized by adequate statistics; all that also requires an X-ray detector with the best possible energy resolution;
- the X-ray peaks must be automatically processed in such a manner to minimize the errors related to their areas; this point is extremely critical, and the currently existing software, generally adequate to process X-ray spectra, are often not sufficient to determine the peak areas in a proper manner. A new more accurate software would be required.

Acknowledgements The research has been supported by Regione Sardegna, 'Progetto di ricerca di base Legge 7/2007, Bando 2008, Studio e realizzazione di sistemi di calcolo scientifico paralleli a basso costo basati su processori grafici, CUP: J71J10000070002'.

References

1. R. D'Oriano, Boll. Archeol. **46–48**, 1 (1997)
2. R. Cesareo, A. Brunetti, S. Ridolfi, X-Ray Spectrom. **37**, 309 (2008)
3. R. Cesareo, M.A. Rizzutto, A. Brunetti, D.V. Rao, Nucl. Instrum. Methods Phys. Res. B **267**(17), 2890 (2009)
4. R. Cesareo, A. Brunetti, J. X-ray Sci. Technol. **16**(2), 119–130 (2008)
5. R. Cesareo, Il. Nuovo Saggiatore **19**, 74 (2003)
6. R. Cesareo, Nucl. Instrum. Methods Phys. Res. B **211**, 133 (2003)
7. R. Cesareo, A. Brunetti, A. Castellano, M.A. Rosales, Portable equipment for X-ray fluorescence analysis, in *X-Ray Spectrometry: Recent Technological Advances*, ed. by K. Tsuji, J. Injuk, R. Van Grieken (Wiley, New York, 2004), pp. 307–341
8. R. Cesareo, X-ray spectrometry, in *Encyclopedia for Industrial Chemistry* (Wiley-Ullmann, New York, 2010)
9. AMPTEK Inc., 6 De Angelo Drive, Bedford, MA 01730-2204, USA. www.amptek.com
10. A. Brunetti, Comput. Phys. Commun. **184**, 573 (2013)
11. G.M. Ingo, E. Angelini, G. Bultrini, T. De Caro, L. Pandolfi, A. Mezzi, Surf. Interface Anal. **34**, 328 (2002)
12. U. Bottigli, A. Brunetti, B. Golosio, P. Oliva, S. Stumbo, L. Vincze, P. Randaccio, P. Bleuet, A. Simionovici, A. Somogyi, Spectrochim. Acta, Part B, At. Spectrosc. **59**, 1747 (2004)
13. A. Brunetti, M. Sanchez del Rio, B. Golosio, A. Simionovici, A. Somogyi, Spectrochim. Acta B **59**, 1725 (2004)
14. T. Schoonjans, A. Brunetti, B. Golosio, M. Sanchez Del Rio, V.A. Solé, C. Ferrero, L. Vincze, Spectrochim. Acta B **66**, 776 (2011)
15. G. Piga, G. Solinas, T.J.U. Thompson, A. Brunetti, A. Malgosa, S. Enzo, J. Archaeol. Sci. **40**, 778 (2013)
16. R. Cesareo, A. Castellano, G. Buccolieri, S. Quarta, M. Marabelli, P. Santopadre, M. Ioele, A. Brunetti, Nucl. Instrum. Methods Phys. Res., Sect. B, Beam Interact. Mater. Atoms **213**, 703 (2004)
17. R. Cesareo, A. Brunetti, X-Ray Spectrom. **37**, 260 (2008)
18. G. Piga, A. Santos-Cubedo, A. Brunetti, M. Piccinini, A. Malgosa, E. Napolitano, S. Enzo, Palaeogeogr. Palaeoclimatol. Palaeoecol. **310**(1–2), 92 (2011)
19. G. Piga, A. Santos-Cubedo, S. Moya Solà, A. Brunetti, A. Malgosa, S. Enzo, J. Archaeol. Sci. **36**, 9 (1857) (2009)